Chapter 4

Fatigue Crack Growth Rate Investigation of Cold rolled and aged Al-Mg-Zn alloy

4.1 Introduction

This research explored the fatigue crack growth rate (FCGR) characteristics correlating with microstructure of Solution heat treated (SHT), SHT+ peak aged (PA), SHT+45% cold rolled (CR), SHT+ 60% warm rolled (WR) and SHT+PA+90% CR Al-Mg-Zn alloy. The findings indicate that artificial aging and cold rolling process decelerate fatigue crack initiation because of precipitation hardening and work hardening as well as grain boundary strengthening, respectively. Utilizing the Paris model, fatigue crack growth rates during the linear extension stage were analyzed. Analysis of crack paths via scanning electron microscope (SEM) techniques revealed ductile fracture(dimples) in case of SHT and SHT+60% WR sample, while ductile and brittle mix fracture (dimples and facets) in case of SHT+PA and SHT+ 45% CR sample, whereas brittle fracture (river pattern, facets) in case of SHT+PA+90% CR sample were observed. The broadening of precipitate peaks in the X-ray diffraction (XRD) graph of SHT+ PA+ 90% CR indicates a rise in dislocation density which is 11.1 $\times 10^{14}\, m^{-2}$. The microstructural evolution is characterized using optical -microscopy, EBSD and transmission electron microscopy (TEM) techniques. Rod like shape η" precipitates were observed in TEM images in the case of SHT+PA+90% CR sample. Through the partition of IPF image it was observed that higher volume fraction of recrystallized grains was formed in SHT+60% WR sample, whereas nano-meter to micrometer size sub grains were formed in the case of SHT+PA+90% CR sample. It was observed through orientation distribution function that SHT+45% CR is showing strong brass

({110}<112>) texture, whereas SHT+60% WR sample is showing strong rotated cube({001}<110>) texture, while 90% CR sample is showing strong brass({110}<112>), strong Cu({112}<111>) and strong S({123}<634>) texture. Mechanical properties are assessed through tensile, hardness, and fracture tests. The highest values for Vickers hardness (226 HV), tensile strength (526 MPa), and conditional elastic-plastic fracture toughness (J_Q) (344.54 kJ/m²) were obtained after SHT (470°C) for a duration of 8 hours), PA (140°C for a duration of 21 hours) and 90% CR.

4.2. Metallography investigation

4.2.1 XRD

The XRD peaks of SHT+ 45% CR and SHT+ 60% WR are identical, whereas in the SHT+ PA+ 90% CR sample, significant peak broadening of the high atomic density plane (111) is evident(Fig.4.1). Precipitate peak of η"(Mg_2Zn_3) is observed in SHT+ PA+ 90% CR sample (Fig.4.1). This broadening is attributed to the high dislocation density. To find the dislocation density following equation is used

$$\rho = \frac{3\sqrt{2\Pi}}{Db}\varepsilon^{(\frac{1}{2})} \quad (4.1)$$

Where ρ= dislocation density

ε = micro strain

D = coherent domain size

b = Burger vector which is $\frac{a}{\sqrt{2}}$

The micro strain (ε) and coherent domain size (D) were determined with the help of "Williamson–Hall" method, as detailed in the literature [84].

Table 4.1 is showing micro strain and dislocation density of SHT+45% CR, SHT+60% WR and SHT+ PA+ 90% CR samples

Table 4.1 micro strain and dislocation density of SHT+45% CR, SHT+60% WR and SHT+ PA+ 90% CR samples

Conditions	Calculated ε (10^{-3})	Calculated ρ ($10^{14}\ m^{-2}$)
SHT + 45% CR	1.7	2.4
SHT+60% WR	1.3	1.9
SHT+ PA+ 90% CR	9.5	11.1

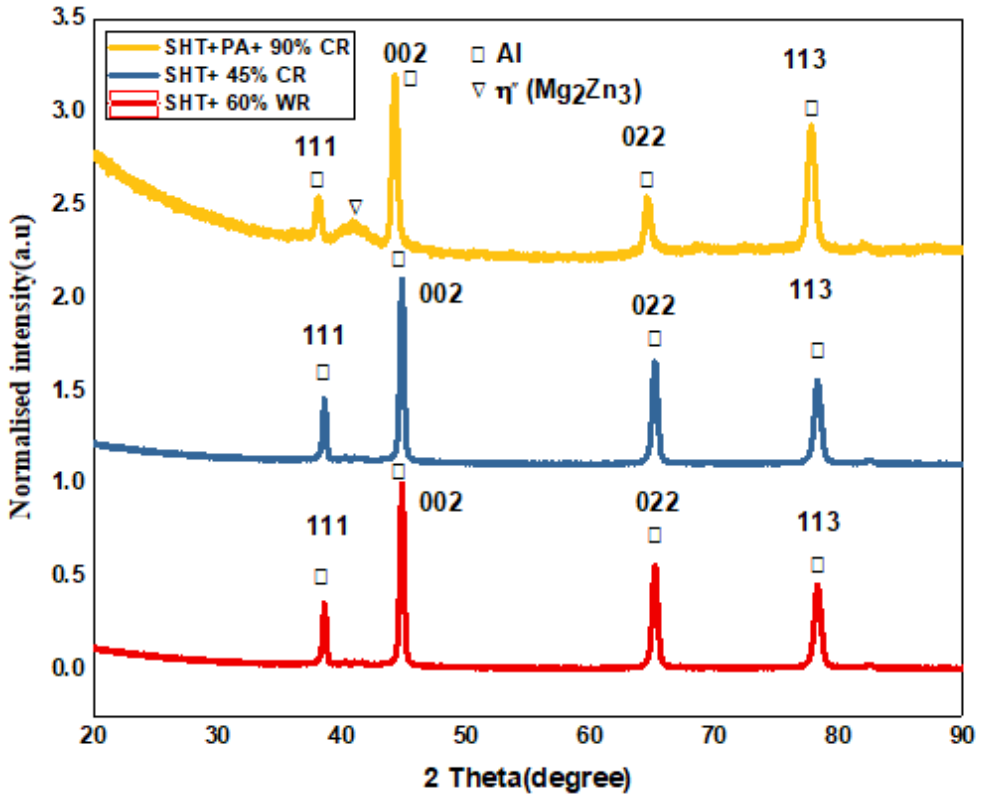

Fig. 4.1 XRD peaks of SHT+ 45% cold rolled, SHT+ 60% warm rolled and SHT+PA+ 90% cold rolled cold rolled sample

4.2.2 Optical- microscopy

Fig. 4.2(a) is showcasing the optical image of the SHT sample where no dispersoids on grain boundary and size of the grain is 51 µm[124], Fig. 4.2(b) is illustrating the SHT+PA image of 7075 Al alloy in which dispersoids are observed on

grain boundary. Size of the grain is 21 µm[124]. Image 4.2(c) is SHT+PA image of 7075 Al alloy at higher magnification to see the dispersoids clearly. Image 4.2(d) is "image quality(IQ)" map of SHT+45% CR sample in which sample is kept its original grain structure with small amount of strain accumulation and deformation bands can be seen on some part of the grains. In this, area fraction of less than 10 µm grains are very small (less than 5%)while area fraction of more than 10 µm grains are high(30%)(Fig.4.2(g)). Image 4.2(e) is IQ map of SHT+ 60% WR sample in which grains are completely fragmented and new fine grains(size less than 10 µm) are formed. From Fig. 4.2(h) its is clear that area fraction of less than 10 µm grains is higher(10%) while arear fraction of less than 100 µm grains is very less(less than 5%). Image 4.2(f) is IQ map of SHT+ PA+ 90% CR sample in which maximum strain accumulation can be seen and some grains are completely fragmented in small grains while some grains are kept its original structure and from Fig 4.2 (i) it is clear that area fraction of less than 10 µm grains lower (8%) than SHT+ 60% WR sample and greater than 100 µm grains is higher (16%) than SHT+ 60% WR sample.

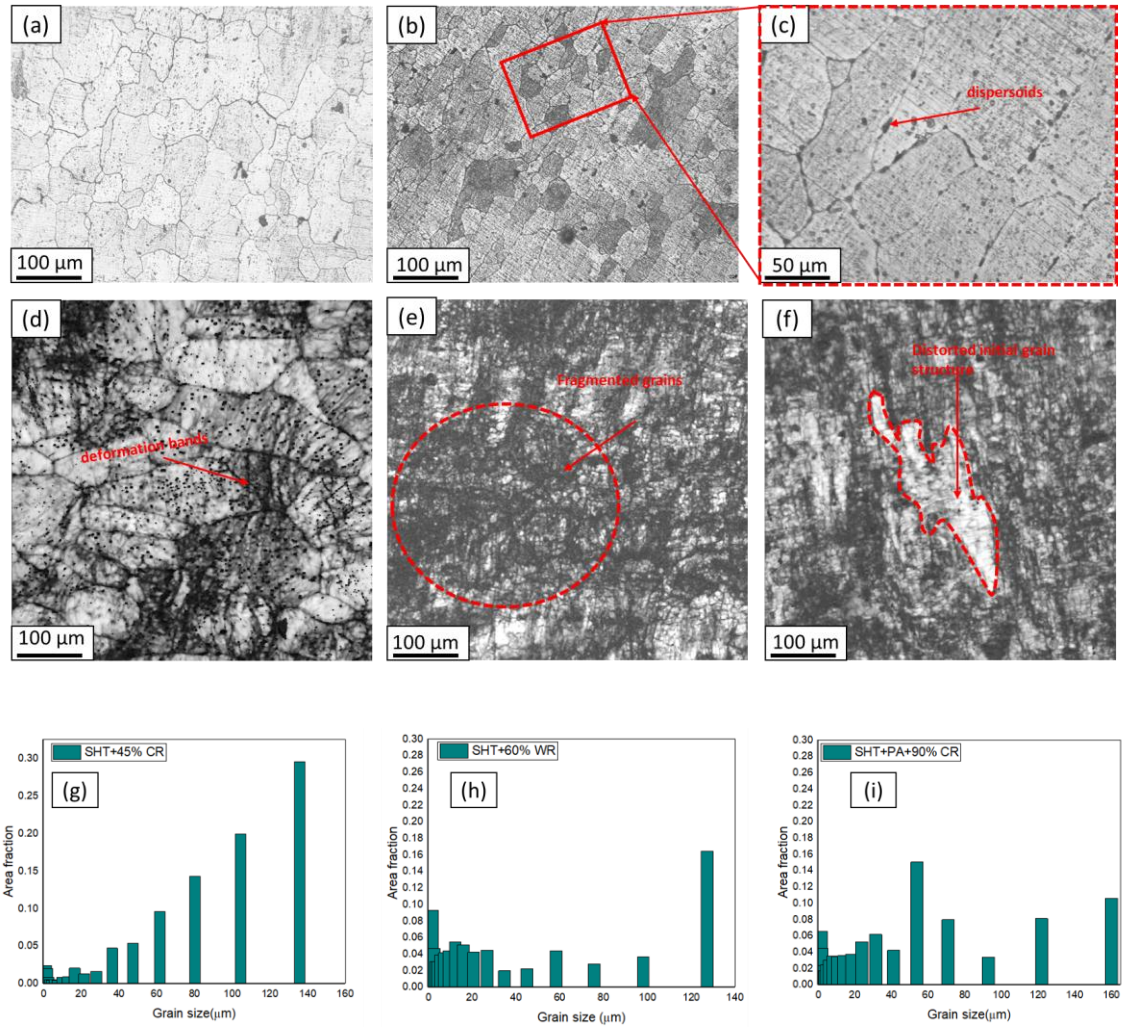

Fig. 4.2 optical image of (a) SHT sample, (b) SHT+ SHT+PA sample at lower magnification, (c) SHT+ SHT+PA sample at lower magnification, (d) IQ image of SHT+ 45% CR sample, (e) IQ (image quality) image of SHT+ 60% WR sample, (f) IQ image of SHT+ PA+ 90% CR sample, (g, h, i) grain size bar chart for SHT+ 45% CR, SHT+ 60% WR, SHT+ PA+ 90% CR

4.2.3 TEM

Rod type shape of precipitates can be clearly investigated in TEM image of the SHT+PA sample clearly illustrated in Fig 4.3(a, b,). In Fig. 4.3(a) white color rod type shape is nothing but the η", which can be clearly seen in Fig. 5(b). From Fig. 4.3(a, b) it is quite clear that very fine precipitates in the range of nanometer is formed which

size is determined with the help of ImageJ software. The calculated average length of the precipitate is 1.8 nm and width is 1 nm. Fig. 4.3(c) is the SAED pattern of Fig. 4.3(b) in which superlattice spots of η" (Mg_2Zn_3) can be observed very clearly

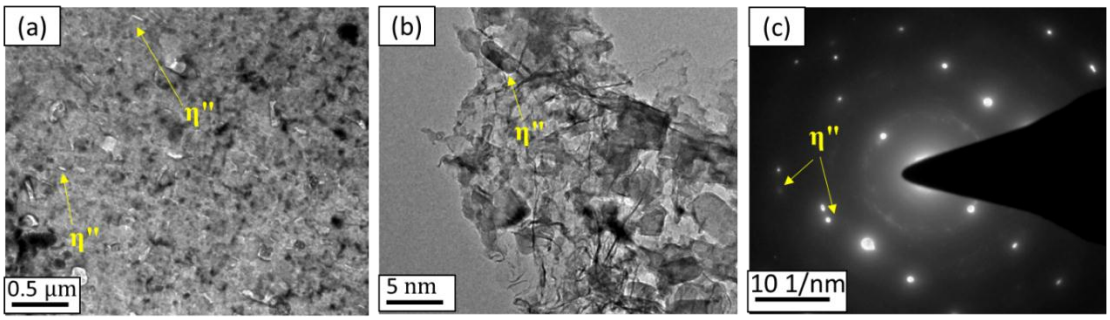

Fig. 4.3 (a) SHT+ PA sample TEM picture at lower magnification, (b) higher magnification TEM image of SHT+ PA sample and (c) is SAED pattern of image (b).

4.2.4 EBSD

Fig. 4.4 and 4.5 are showing the IPF and Kernel Average Misorientation (KAM) image of SHT+45% CR, SHT+60% WR and SHT+PA+90% CR samples respectively. In which it is clearly observed that SHT+PA+90% sample is highly deformed as compared to SHT+60%WR sample and SHT+45% CR sample.

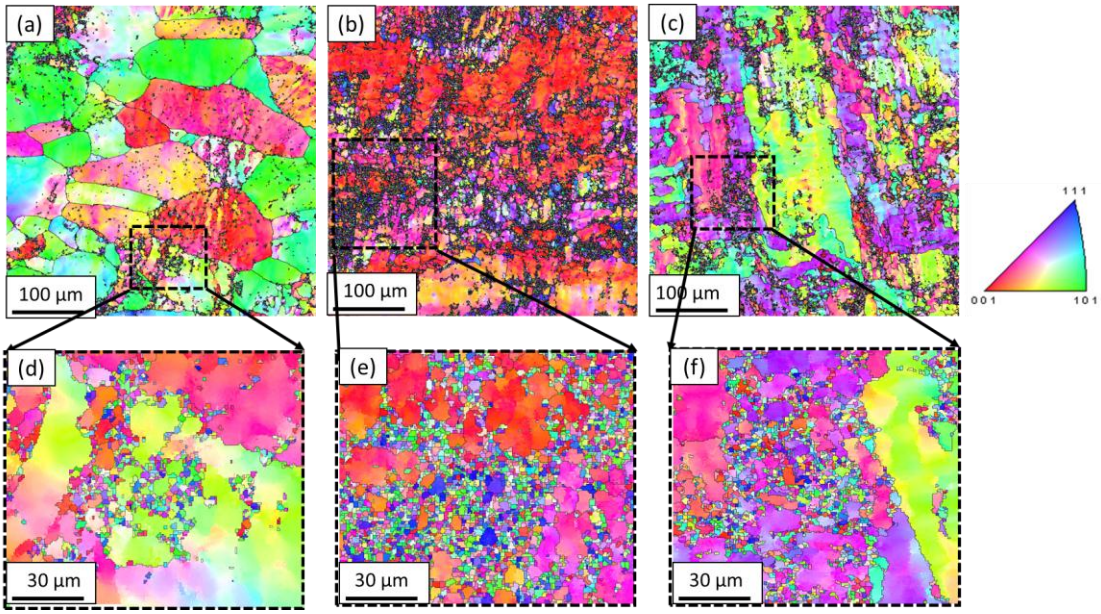

Fig.4.4 (a, b, c) IPF image of SHT+45% CR, SHT+60% WR and SHT+PA+90% CR samples, (d, e, f) higher magnification image of a, b, c respectively.

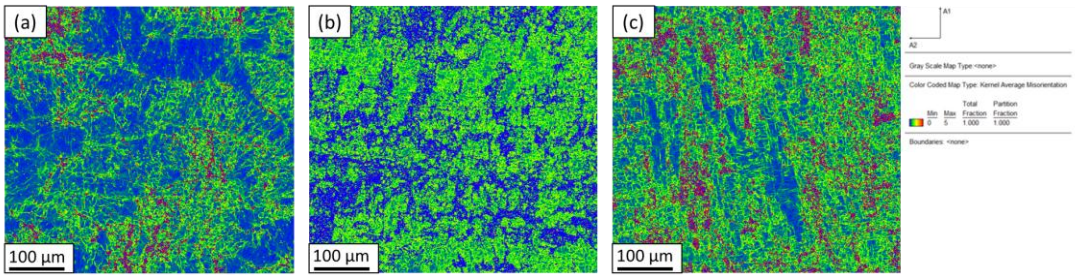

Fig.4.5 (a, b, c) Kernel Average Misorientation (KAM) image of SHT+45% CR, SHT+60% WR and SHT+PA+90% CR samples

In Fig. 4.6 since blue color part is more visible than red and green color part in all three images (a, b, c), which is confirming the emergence of high angle grain boundary within all three conditions and it is maximum visible in Fig. 4.6(b) which signifies the formation of high angle grain boundary (stable grain) is maximum in SHT+ 60% WR sample than in SHT+PA+90% CR sample and minimum in SHT+ 45% CR sample.

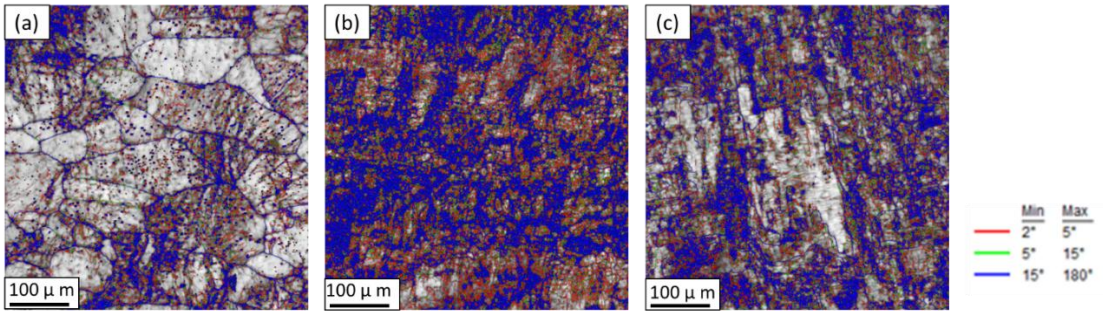

Fig. 4.6 Image quality (IQ) map of (a) SHT+45% CR, (b) SHT+60% WR and (c) SHT+PA+90% CR samples

From Fig. 4.7 it is confirmed that recrystallize grain with high angle grain boundary is more in SHT+ 60% WR sample (Fig. 4.7(b)) and minimum in SHT+ 45% CR sample while moderate in SHT+ PA+ 90% CR sample.

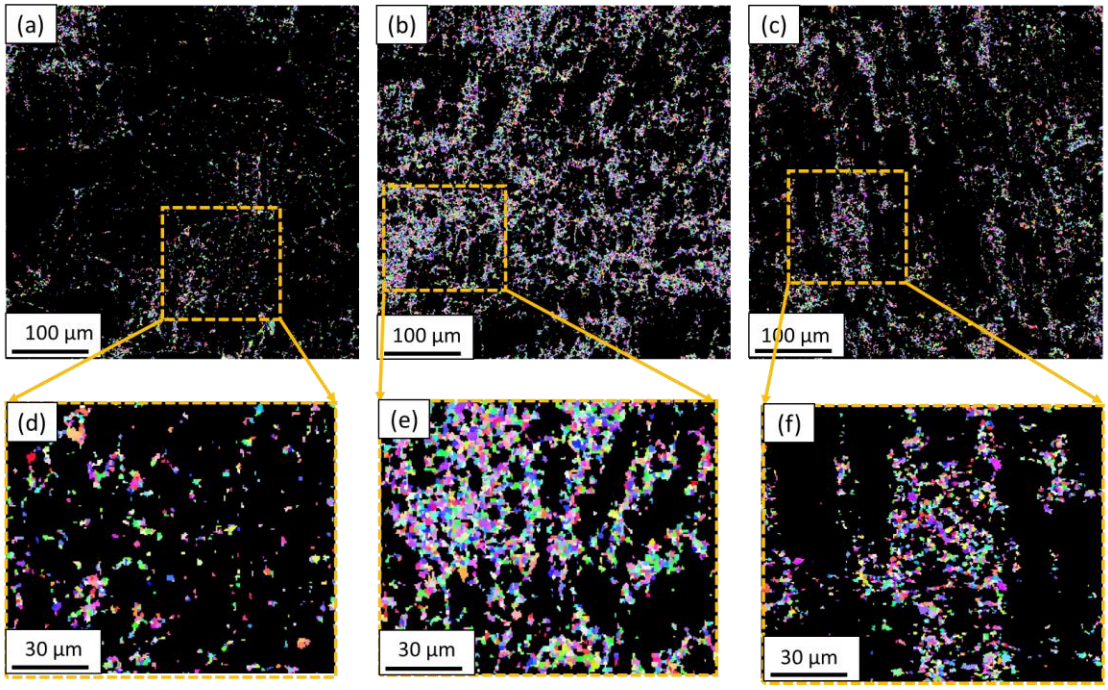

Fig. 4.7 Using the criteria GOS < 1° and limit misorientation > 15°, the IPF-image was partitioned to determine the recrystallized-grains of (a)SHT+ 45% CR, (b) SHT+60% WR, and (c) SHT+ PA+ 90% CR. (d, e, f) higher magnification image of a, b, c respectively.

In Fig. 4.8 sub- grains are illustrated with low angle grain boundary which is minimum in SHT+ 45% CR sample and maximum in SHT+ PA+ 90% CR sample and moderate in case of SHT+ 60% WR sample. Very small size (range of nm) sub-grains are formed in SHT+ PA+ 90% CR sample (Fig.4.8(c)) while large size (range of µm) is found in SHT+ 60% WR sample (Fig.4.8(b))

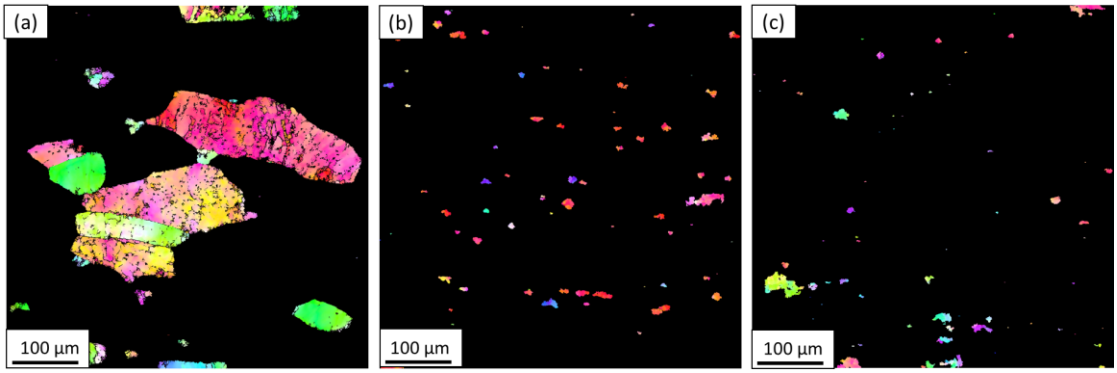

Fig. 4.8 To determine the sub-grains, the IPF-image is partitioned using the criteria GOS > 2° and 2°< limit misorientation < 15°(a) SHT+45% CR, (b) SHT+60% WR, and (c) SHT+ PA+ 90% CR3

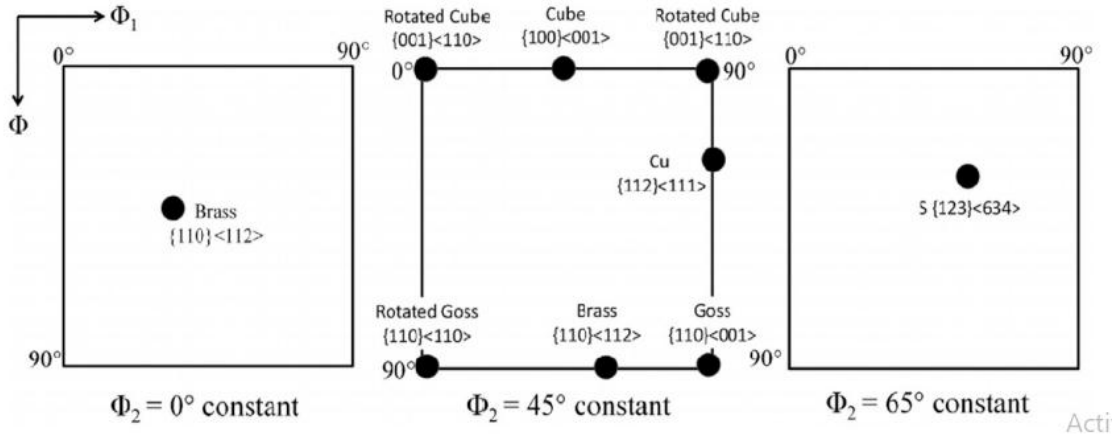

Fig. 4.9 The φ2 at 0°, 45°, and 65° sections of the orientation distribution function (ODF) illustrate the standard components that are typically observed in face-centered cubic (FCC) metals and alloys [125]

Fig. 4.9 is representing the standard components which can be typically seen in FCC materials.

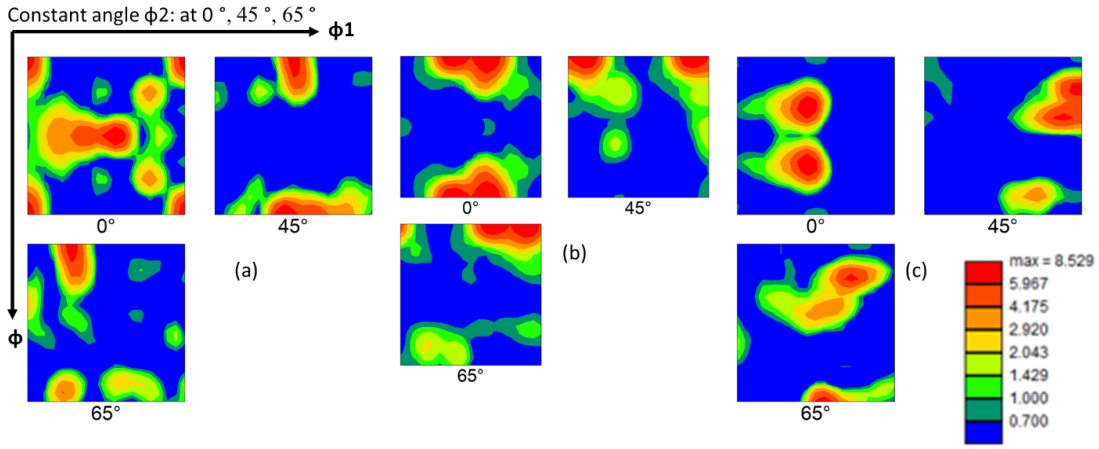

Fig. 4.10 Texture image of (a) SHT+45% CR, (b) SHT+60% WR and (c) SHT+PA+90% CR samples

Accordance with the Fig.4.10 SHT+45% CR is showing strong brass ({110}<112>) texture whereas SHT+60% WR sample is showing strong rotated cube({001}<110>) texture, while 90% CR sample is showing strong brass({110}<112>), strong Cu({112}<111>) and strong S({123}<634>) texture.

4.3 Mechanical testing

4.3.1 Vickers Hardness test

Vickers hardness of all 5 conditions is shown in Fig. 4.11. In which average hardness of SHT, SHT+ PA, SHT+45%CR, SHT+60%WR and SHT+PA+90%CR are 128,195,177,170 and 224 HV respectively

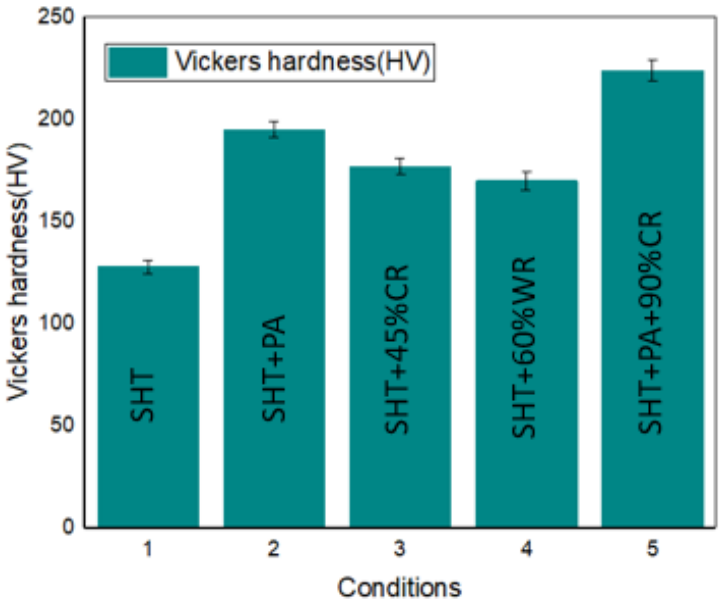

Fig 4.11 Hardness test of SHT, SHT+ PA, SHT+45% CR, SHT+60% WR, SHT+PA+90%CR

4.3.2Tensile test

The ultimate tensile strength (UTS), yield strength (YS), and percentage elongation of as received, SHT, SHT+ SHT+PA, SHT+ 45% CR, SHT+ 60% WR, and SHT+PA+90% CR were all determined via a tensile test. Table 4.2 is displaying the results of tensile test for all five conditions samples and Fig. 4.12 is showing one of the tensile test results graphs.

Table 4.2: tensile test result for as received, SHT, SHT+ PA, SHT+ 45% CR, SHT+ 60% WR, SHT+SHT+PA+90% CR respectively.

Conditions	**YS(MPa)**	**UTS(MPa)**	**% elongation**
As received	375.8±5	462.8±5	11±1%
SHT	150±10	170±10	12±2%
SHT+ PA	450±10	496.5±10	8±3%
SHT+ 45% CR	280±5	350± 5	9±2%,
SHT+ 60% WR	180±10	285± 10	12±4%
SHT+SHT+PA+90% CR	480±5	526±5	6± 3%

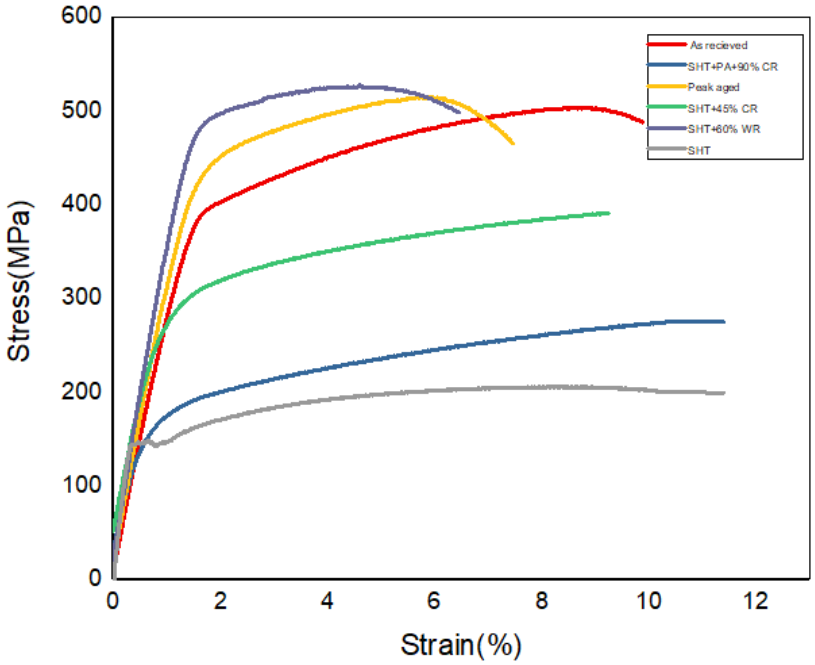

Fig. 4.12 Tensile test result of as received, SHT, SHT+ PA, SHT+45% CR, SHT+60% WR and SHT+PA+90% CR samples

4.3.3 Fatigue Crack Growth Rate (FCGR) test

Fatigue crack growth rate for SHT, SHT+PA, SHT+45% CR, SHT+60% WR and SHT+PA+90% CR are shown in Fig. 4.13. Threshold value of ΔK for SHT is 5.9 MPa√m, for SHT+45% CR is 9 MPa√m, for SHT+60% WR is 7.9 MPa√m, for SHT+PA is 10 MPa√m and for SHT+ PA+ 90% CR is 12 MPa√m. From the threshold value of SHT, SHT+ SHT+PA, SHT+45% CR, SHT+60% WR and SHT+PA+90% CR samples it is clear that crack initiation in SHT is faster as compared to aged, SHT+45% CR, SHT+60% WR and SHT+PA+90% CR samples. Threshold value for 90% rolled sample is maximum in all these three conditions, which showing that crack initiation starting comparatively late in this case. The purpose of Fig. 4.13 is to identify and differentiate the all three regions of FCGR (crack initiation, crack propagation and unstable crack growth) of all five conditions clearly. No. of cycles for all five conditions

are given in Table no. 4.3 which is calculated with the help of equation 3[8]. Firstly, C and M are calculated by the linear fitting of stable crack growth region using the equation no. 4.2[8]. Afterwards their values are substituted in equation 4.3 to find the no. of cycles for each condition.

$$\frac{da}{dN} = C\,\Delta K^m \tag{4.2}$$

m and C are the material constants

$\frac{da}{dN}$ is rate of crack growth

ΔK = Stress intensity factor range

$$N_f = \frac{[2(ac^{\left(\frac{2-m}{2}\right)} - ai^{\left(\frac{2-m}{2}\right)})]}{(2-m)C\Delta K^m} \tag{4.3}$$

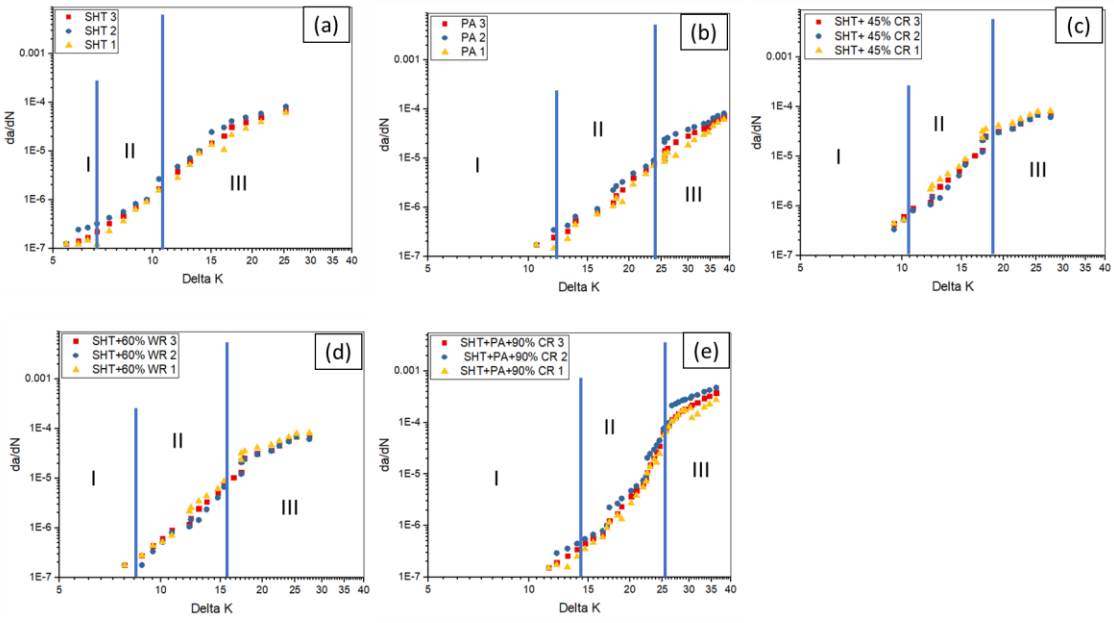

Fig. 4.13: (a, b, c, d, e) Paris law for SHT, SHT+ PA, SHT+45% CR, SHT+60% WR and SHT+PA+90% CR samples

Table 4.3: No. of cycles for all five conditions with as received condition.

Conditions	SHT	SHT+PA	SHT+45% CR	SHT+60%WR	SHT+PA+90% CR	As received
No. of cycles (N)	111790	336341	266352	143003	454995	340000[126]
C	6.849×10^{-8}	8.654×10^{-13}	5.329×10^{-12}	9.217×10^{-11}	7.534×10^{-15}	4.3316×10^{-9} [126]
M	4.543	1.985	2.649	3.789	1.825	1.912[126]

4.3.4 Conditional Elastic-Plastic (J_Q) fracture test

The load point displacement technique analysis, previously covered in our research paper [124], was used to assess the elastic plastic fracture toughness (J_1c) of all five conditions samples. In order to confirm the elastic-plastic fracture toughness the minimum unbroken ligament (b) and thickness (B) needed were found to be "17.394" mm for SHT+ PA+ 90% CR, "16.34" mm for SHT+PA, and "13.5" mm for SHT[124]. Similarly, b and B are computed for SHT+45% CR and SHT+60% WR in the current study. The results show that B for SHT+45% CR is 15.12 and for SHT+60% WR is 14.58 mm. In this study, the sample thickness was 5.7 mm, and the unbroken ligament measured 25.4 mm. Therefore, the calculated "B" values for the PA, SHT, SHT+45% CR, SHT+60% WR, and SHT+PA+90% CR samples did not satisfy the conditions specified in Eq. (3.6). Since both thickness requirements were not fulfilled and the preparation of this thick sample was difficult, the computed plane stress fracture toughness for the SHT+PA+90% CR, SHT, SHT+PA, SHT+45% CR, SHT+60% WR, and SHT+PA+90% CR samples reflect a conditional fracture toughness (J_Q). Table 4.4 lists the conditional fracture toughness for each of the five conditions. Fig. 4.14 illustrating the load point displacement curve for all five conditions.

Table 4.4: Conditional fracture toughness for SHT, SHT+PA, SHT+45% CR, SHT+60% WR and SHT+PA+90% CR samples

Samples	Conditional fracture toughness (J_Q) (kJ/m2)
SHT	82.5±5
SHT+PA	230.35±7
SHT+45% CR	180± 5
SHT+60% WR	150± 5
SHT+PA+90% CR	344.54±10

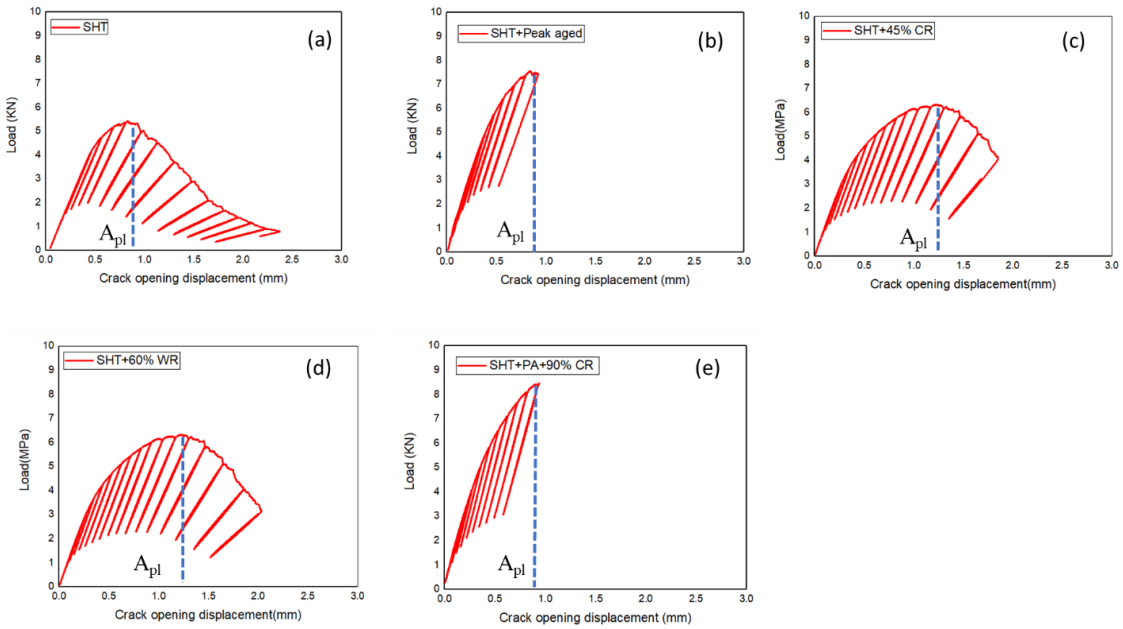

Fig 4.14 Load vs displacement graph for SHT, PA, SHT+45% CR, SHT+60% WR, SHT+PA+ 90% CR.

4.4 Fractography

Fractography of SHT, SHT+PA, SHT+45% CR, SHT+60% WR and SHT+PA+90% CR samples are shown in following figure, the two regions pre-crack and final fracture can be clearly observed in Fig. 4.15. Figs. 4.16,4.17,4.18, 4.19 and 4.20 are the globular view of fatigue pre crack area with all three regions of (crack initiation, crack propagation, unstable crack growth region).

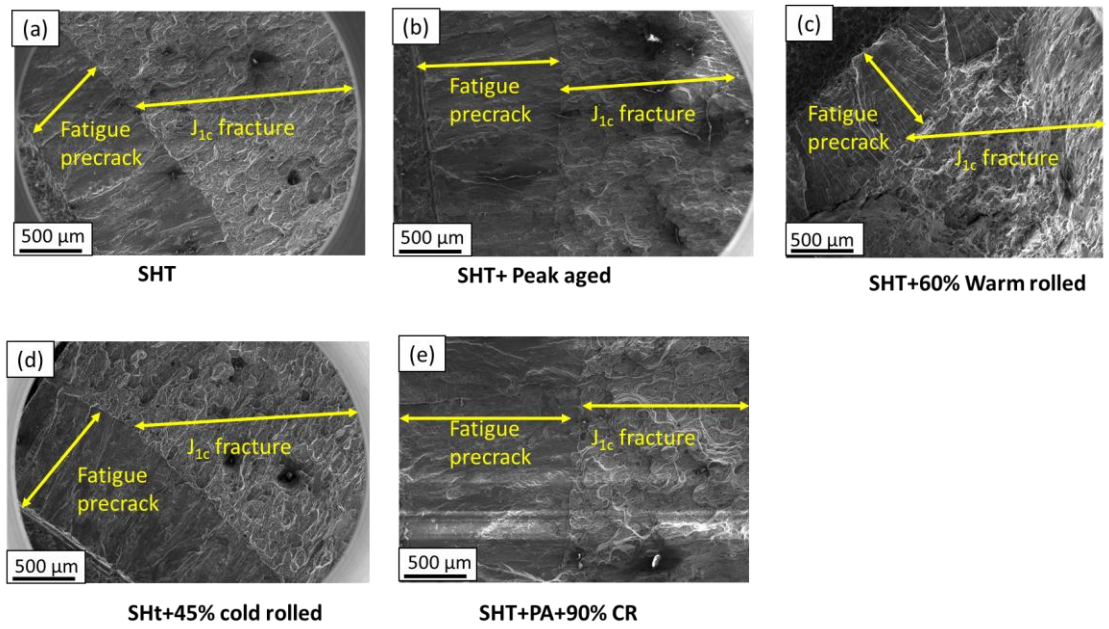

Fig 4.15 Pre-crack and final fracture for SHT, SHT+PA, SHT+45% CR, SHT+60% WR and SHT+PA+90% CR samples

4.4.1 Fatigue crack growth rate (FCGR) test

The three stages of FCGR initiation(I), propagation (stable crack growth) (II) and unstable crack growth (III) are clearly illustrated in the fractography images for all five conditions (SHT, peak-aged, SHT+45% CR, SHT+60% WR and SHT+PA+90% CR) in figs. 4.16–4.20. Fig. 4.16 is fatigue crack growth (FCG) region of SHT sample in which crack initiation and propagation portion is small (Fig. 4.16(a)) and fatigue ridges are openly packed (Fig.4.16(c)). Fig.4.17 is FCG region of SHT+PA sample wherein crack initiation zone is larger than SHT (Fig. 4.16(a)), and fatigue ridges are densely packed than SHT (Fig.4.16 (c)). Fig. 4.18 is FCG region of SHT+ 45% cold rolled sample in which crack initiation part is more as compared to SHT and SHT+60% WR sample (Fig.4.19) but less than SHT+PA and SHT+ PA+ 90% CR sample (Fig. 4.20). Fig. 4.21 and Fig. 4.22 are displaying the stable crack growth region and unstable crack growth region respectively for all five conditions where striations are clearly visible in

the perpendicular direction of crack growth direction. In Fig. 4.21 (stable crack growth) striations are fine whereas in Fig. 4.22 (unstable crack growth) striations are wide. Striation length is larger in SHT sample (Fig. 4.21(a), Fig. 4.22(a)) while length of striation is smaller in SHT+ PA+ 90% CR sample (Fig. 4.21(e), Fig. 4.22(e)).

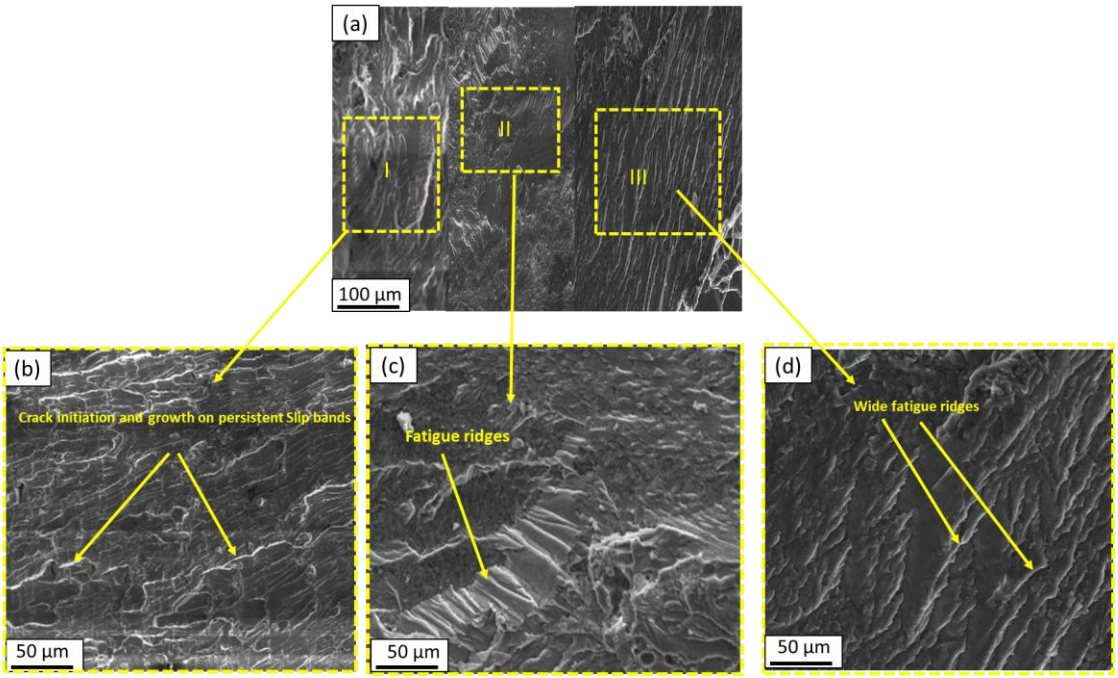

Fig. 4.16 (a) SHT sample globular view of pre crack area with all three regions of (b) crack initiation, (c) crack propagation, (d) unstable crack growth region

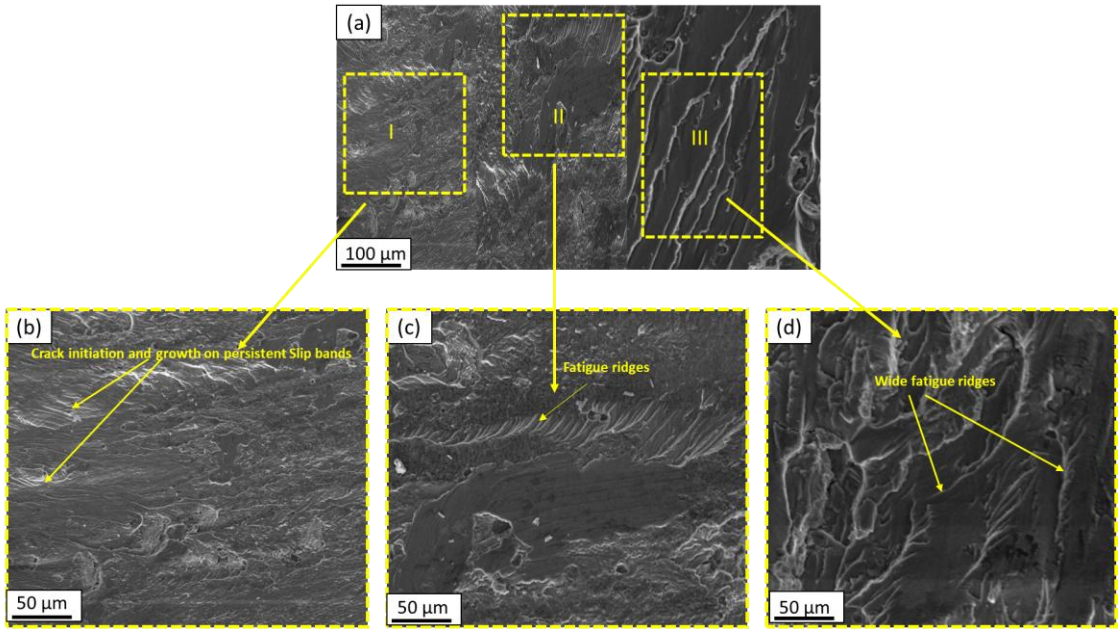

Fig. 4.17 (a) SHT+PA sample globular view of pre crack area with all three regions of (b) crack initiation, (c) crack propagation, (d) unstable crack growth region

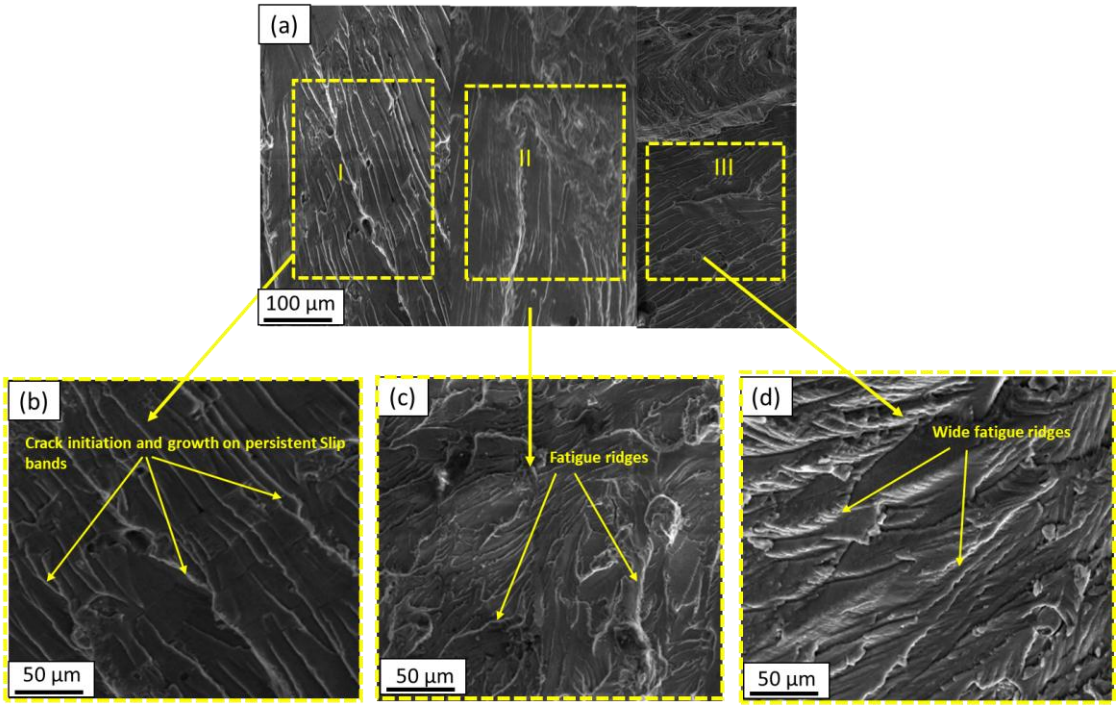

Fig. 4.18 (a)SHT+ 45% CR sample globular view of pre crack area with all three regions of (b) crack initiation, (c) crack propagation, (d) unstable crack growth region

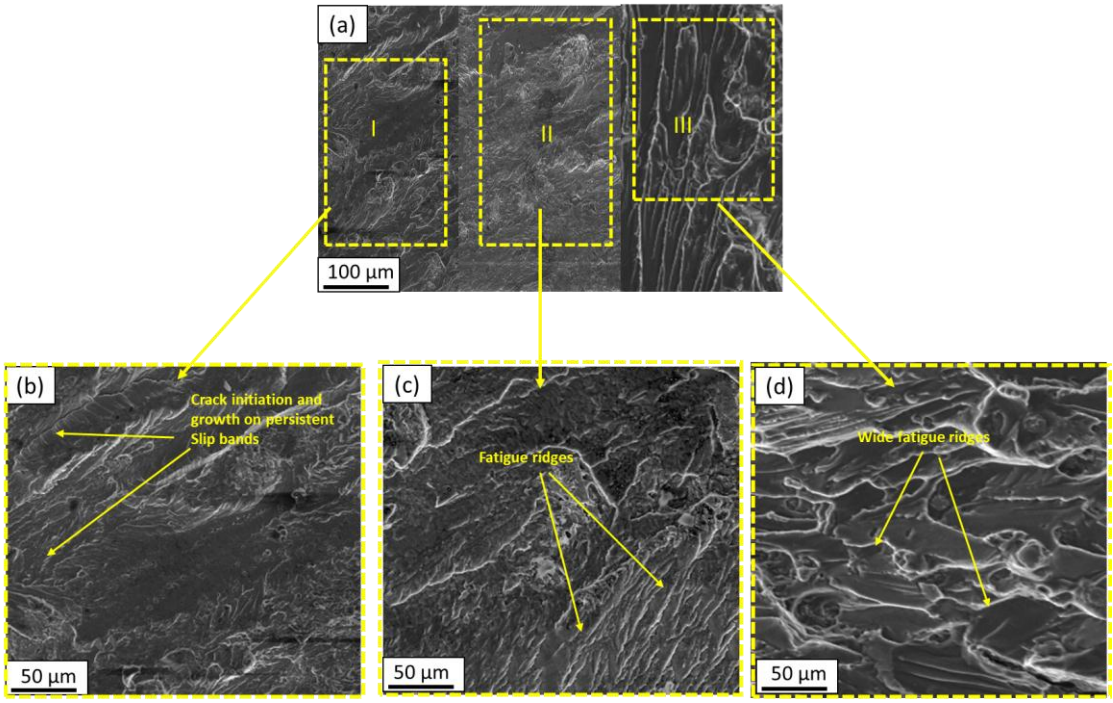

Fig. 4.19 (a) SHT+ 60% WR sample globular view of pre crack area with all three regions of (b) crack initiation, (c) crack propagation, (d) unstable crack growth region

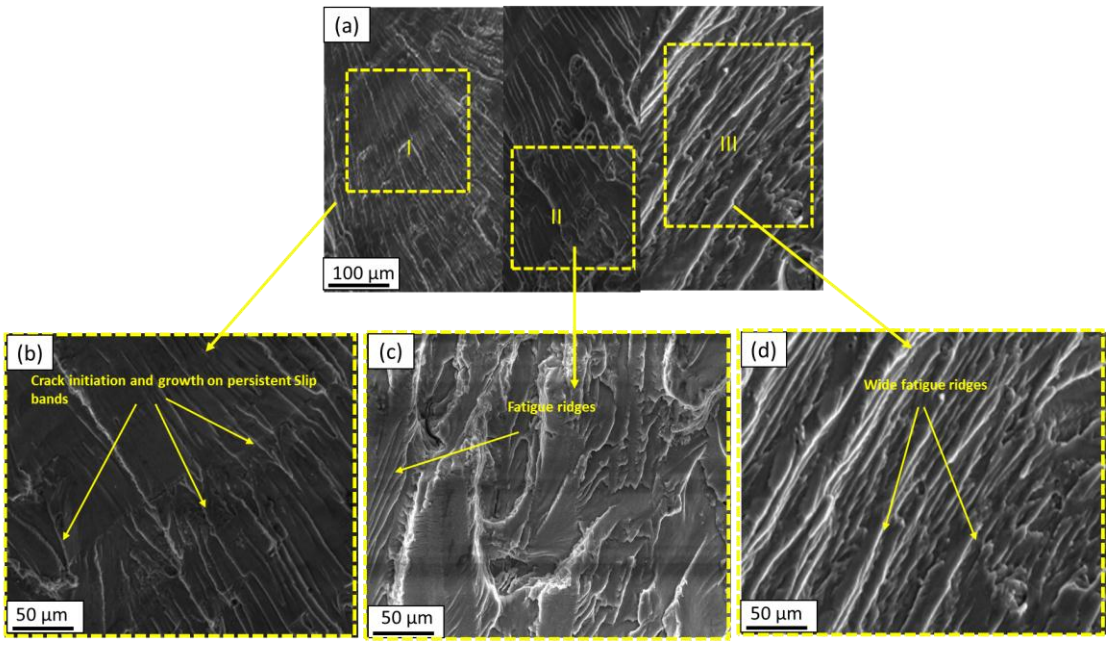

Fig. 4.20 (a) SHT+ PA+ 90% CR sample globular view of pre crack area with all three regions of (b) crack initiation, (c) crack propagation, (d) unstable crack growth region

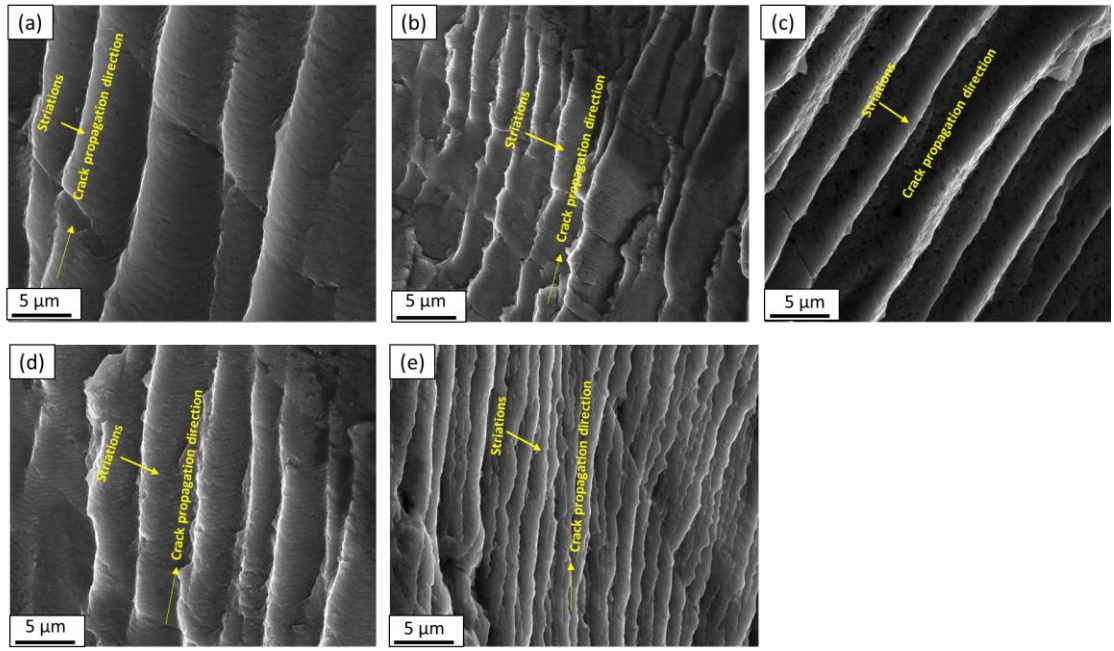

Fig. 4.21 stable crack growth region for (a)SHT, (b) SHT+PA, (c)SHT+45% CR, (d)SHT+60% WR and (e) SHT+PA+90% CR samples

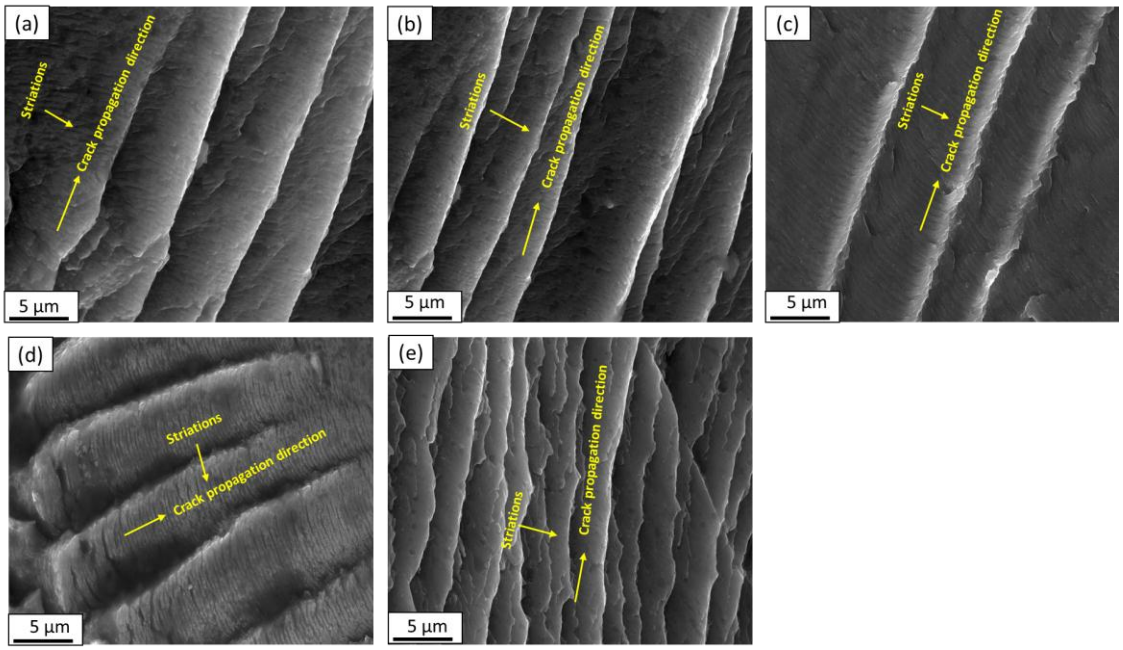

Fig. 4.22 Unstable crack growth region for (a)SHT, (b) SHT+PA, (c)SHT+45% CR, (d)SHT+60% WR and (e) SHT+PA+90% CR samples

4.4.2 Conditional Elastic-Plastic (J_Q) fracture test

Fig. 4.23 presents the fractography images of samples under all five conditions before $P_{max.}$ Fig. 4.23(a) shows the fractography of the SHT sample, where cracks propagate along the grain boundaries (intergranular failure), and voids are visible on the surface. In Fig. 4.23(b), which corresponds to the SHT+PA condition, both micro-voids and facets are present on the fracture surface. Fig. 4.23(c) displays the fractography of the SHT+45% CR sample, revealing trans granular failure, along with the presence of both micro-voids and facets on the fracture surface. Fig. 4.23 (d) illustrates the fractography of the SHT+60% WR sample, where cracks propagate along the grain boundaries, and small voids are observed on the surface. Finally, Fig. 4.23(e) depicts the fractography of the SHT+PA+90% CR sample, where trans granular failure dominates, and a river-like pattern is observed on the surface. Fracture features such as dimples, facets, and river patterns are less pronounced before P_{max}.

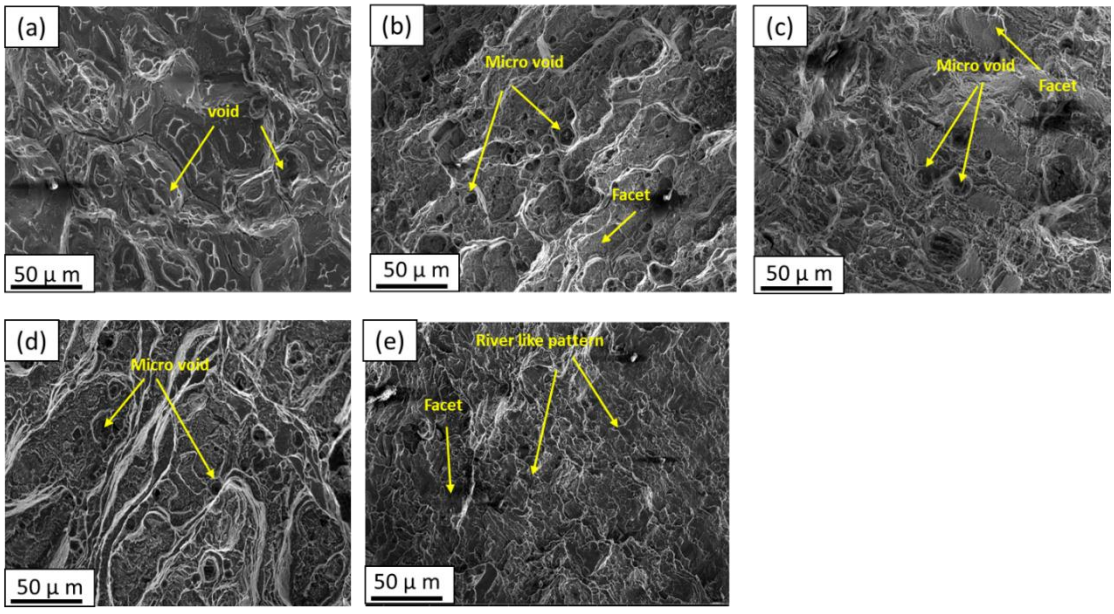

Fig. 4.23 Fractography image of final fracture zone of CT samples before P_{max} of (a)SHT, (b) SHT+PA, (c)SHT+45% CR, (d)SHT+60% WR and (e) SHT+PA+90% CR samples respectively.

Fig. 4.24 presents the fractography images of samples under all five conditions after P_{max}. Fig. 4.24(a) shows the SHT sample, where large dimples are visible on the fractured surface. In Fig. 4.24(b), corresponding to the SHT+PA condition, both dimples and facets are observed on the fractured surface. Fig. 4.24(c) depicts the fractography of the SHT+45% CR sample, showing a mix of dimples and facets, with facets being more prevalent. Fig. 4.24(d) illustrates the fractography of the SHT+60% WR sample, where numerous large dimples dominate the fractured surface. Lastly, Fig. 4.24(e) represents the SHT+PA+90% CR sample, exhibiting both facets and a river-like pattern on the fractured surface. The fracture features like dimples, facets, and river patterns become more pronounced after P_{max}.

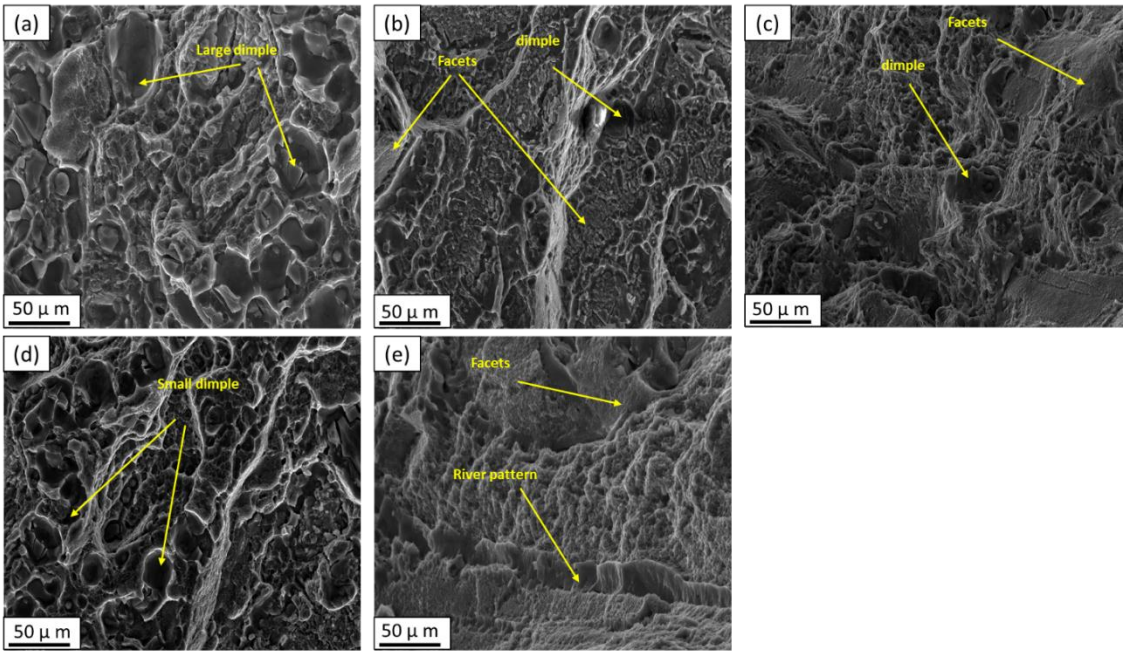

Fig. 4.24 Fractography image of final fracture zone of CT samples after P_{max} of (a)SHT, (b) SHT+PA, (c)SHT+45% CR, (d)SHT+60% WR and (e) SHT+PA+90% CR samples respectively.

4.5 Discussion

4.5.1 Mechanical and Microstructural correlation

Figure 4.1 makes it abundantly evident that the peak of the (111) plane of Al matrix getting broader as the percentage of deformation rises because of the increase in dislocation density [127,128]. The TEM (figs. 4.3(a), (b)) and SAED (Fig. 4.3(c)) pattern analysis demonstrate that fine precipitates of η" (Mg_2Zn_3) are seen at the peak ageing state. The dislocations movement was hindered by these nano size η" precipitates [129,130].The interaction of precipitates with dislocations can be occurred by two mechanism (i) Shearing mechanism, (ii) Bypass mechanism depending on the size of the precipitates[38,115,131]. Critical size of the diameter of precipitates can be calculated by the equation 4.4[95].

$$d_c = \frac{4\Pi G m b}{Gp} \tag{4.4}$$

where G_m and G_p are the shear modulus of matrix and precipitates respectively, and b is the Berger vector. Berger vector for Al is 0.286 nm and shear modulus is 26 GPa and shear modulus of precipitate (Mg_2Zn_3) is 65 GPa [95]. Substituting all these values in equation 4.4, the calculated critical diameter of Mg_2Zn_3-precipitates was found to be 1.95 nm. If the size of precipitates was less than the critical diameter, then precipitates interact with dislocations by shearing mechanism otherwise bypass mechanism will be dominated. In the present study average length of precipitates is 1.8 nm, and average width is 1nm, both are less than 1.95 nm. Therefore, in the present study precipitation strengthening is governed by shearing mechanism, resulting in higher hardness and tensile strength in the SHT+PA sample (Figs. 4.11 and 4.12).

The SHT+ PA+95% CR sample have highest strength of 526±5 MPa (Fig. 4.12), highest average hardness value of 226 HV (Fig.4.11) and highest conditional fracture toughness value of 344.54 kJ/m² (Fig.4.14(e)) among all five condition samples due to the more pronounced strain hardening effect (Fig.4.2(f)) in cold rolling[132]. This is correlated by IPF image, Fig. 4.4(c), which shows that the SHT+PA+90% CR sample is heavily deformed, with a significant formation of sub-grains as shown in Fig. 4.4(c). The strength of SHT+45% CR sample (350± 5 MPa) is higher than SHT+60% WR (285± 10 MPa) sample because cold rolling typically results in higher strength due to greater strain hardening compared to warm rolling (Fig.4.2(e)), where recovery processes reduce the effectiveness of strain hardening[128]. The SHT+60% WR (12±2%,) sample is more ductile than the SHT+45% CR (9±2%,) sample, because recrystallized grains formation in the SHT+ 60% WR sample is greater than the SHT+45% CR sample due to higher temperature of warm rolling which can be clearly observed in figs. 4.5(a, b). Recrystallized grains are maximum in SHT+60% WR sample because of the higher rolling temperature encourages dynamic recrystallization or static recrystallization shortly after deformation, as the atoms have sufficient mobility[133,134]. The textures in rolled samples, observable through ODF studies, depend on the degree of deformation and the temperature during rolling[91]. Textures in SHT+45% CR sample was the strong Brass ({110}<112>) as illustrated in Fig. 4.10(a). Because brass texture is dominant in cold rolled sample[135]**.** The texture observed in SHT+60% WR sample was strong rotating cube ({001}<110>), shown in Fig.4.10(b), due to partial recrystallization[136]. In SHT+PA+90% CR, the deformation textures are very pronounced. The material is predominantly exhibiting strong Brass, Copper, and S textures. The high degree of rolling increases the alignment

of crystallographic planes and directions, making these texture components highly observable[84,125]. Area fraction of more than 10 μm grains are maximum in SHT+45% CR sample and minimum in SHT+60% WR sample while moderate in SHT+PA+90% CR sample because in cold rolling, grains resist fragmentation to some extent due to strain hardening[114] whereas in warm rolling, due to elevated temperature the thermal energy allows for easier movement of dislocations within the crystal lattice[108]. This enhanced dislocation mobility promotes dynamic recrystallization (Fig.4.5(b)) and strain hardening is suppressed by thermal recovery processes, allowing grains to fragment more easily and leads to the formation of new, smaller grains during deformation[128,137].

4.5.2 Fatigue Crack Growth Rate (FCGR)

The three regions were appeared during the FCGR test as described in detail in the below section as follow:

Region I (Crack Initiation or Threshold region): ΔK value is maximum for SHT+PA+ 90% CR sample and minimum for SHT sample. SHT sample is softest in all five conditions samples, therefore crack initiation is easier in SHT sample due to easy formation of persistent slip bands (dislocations move back and forth along specific crystallographic planes, forming highly localized structures called PSBs)[43]. The cyclic motion of dislocations within PSBs leads to irreversible strain, causing surface roughness in the form of extrusions and intrusions. These surface irregularities act as stress concentrators, significantly amplifying the local stress at the microscopic level[8,138]. Fatigue cracks typically initiate at intrusions where tensile stress is maximized, as the material here is highly strained and weakened. The initial crack

propagation often follows a crystallographic path along the slip plane of the PSBs, as this is the plane of maximum shear stress and weakest material resistance[139,140] PSBs (figs. 4.16 (b), 4.17 (b) ,4.18(b), 4.19(b) and 4.20(b)) form more easily in softer materials compared to brittle ones. This is because most of softer materials were having closed packed planes of higher atomic density, allowing dislocations to move and accumulate over time under cyclic loading, which leads to the formation of PSBs and brittle materials tend to resist dislocation motion due to their higher strength, so they are less prone to forming PSBs[140,141] . In SHT+PA sample crack initiation is difficult due to precipitation hardening[24,142], because the precipitates act as barriers to dislocations movement, forcing dislocations to cut through the precipitates by shearing mechanism. This resistance to dislocation motion prevents localized slip from developing into PSBs. [130]. SHT+PA sample ΔK value is 10 MPa$\sqrt{m}$. ΔK value for SHT+PA+90% CR sample was 12 MPa$\sqrt{m}$. The crack initiation was delayed in SHT+PA+90% CR sample as compared all other investigated samples because persistent slip bands formation was difficult due to more dislocation's interaction between the exiting dislocations and new dislocations generated, led to dislocation annihilations and enhance the grain boundary strengthening [82,133,137]. In SHT+PA+90% CR sample dislocations get entangled or pinned, making slip (the movement of dislocations on slip planes) more difficult. This delays the localization of plastic deformation that typically leads delay in PSBs formation[140,143]. Fatigue crack initiation is easier in SHT samples and difficult in the case of SHT+PA+90% CR sample (Fig. 4.13) as described in this section.

Region II (Stable crack growth or crack propagation region): Crack propagation rate in SHT(N=111790), SHT+60% WR(N=143003) sample was rapid as compared to

SHT+45% CR (N=266352), SHT+PA (N=336341) and SHT+PA+90% CR (N=454995) samples (Fig.4.13) might be due to SHT sample has coarse grains(Fig.4.2(a)), and SHT+60%WR sample has large no. of micro-meter size recrystallized (Fig. 4.5 (b)) as well as sub-grains (Fig.4.6(b)) which helps to propagate crack easily along the grain boundaries[8,43,93]. Whereas, in case of SHT+45% CR sample crack propagation is slow due to distorted grains interaction with crack movement[144,145]. In SHT+PA sample crack propagation is difficult because of precipitation interaction with the crack movements [130,146]. In SHT+PA+90% CR sample crack propagation rate is slowest due to precipitation strengthening, strain hardening, grain boundary strengthening and formation of large number of non-uniform small size sub grains of size nanometer to micrometer (Fig.4.6(c)) [20,32,128,137]. Fatigue ridges in SHT and SHT+60% WR sample is openly spaced (figs. 4.21(a) and(d)) while it is densely spaced in SHT+PA, SHT+45% CR and SHT+PA+90% CR samples (figs.4.20 (b), (c) and(e)). Length of striation in SHT is higher than SHT+PA+90% CR sample. Larger length of the striations generally indicates a rapid crack growth rate[140,143]. Shorter length striations, on the other hand, imply a slower crack growth rate, potentially indicating that the sample is still in an early phase of fatigue life where the stable crack growth was occurred. Samples with shorter fatigue striations length typically have a longer fatigue life. Short striations length mean that it takes more cycles for the crack to propagate through the sample, which prolongs the time until failure. Conversely, longer striations length is often associated with samples that have a shorter remaining fatigue life, as they indicate that the crack is progressing more rapidly [8,43,143] like in the case of SHT and SHT+60% WR sample.

Region III (Unstable crack growth region): In this region, the crack growth rate increases rapidly as ΔK approaches the sample's fracture toughness. The sample will eventually fail catastrophically[43,143]. Paris' Law no longer applies in this region because the crack growth becomes highly unstable[138] which can be clearly observed in figs. 4.16,4.17,4.18, 4.19 and 4.20 in which the final region is showing broader fatigue ridges than region II. Fatigue striations is also getting broader in this region due to fatigue loading [95] as shown in Fig. 4.22. The growth rate in the unstable region is significantly higher (Fig.4.13), which means the crack is less constrained and can travel longer distances with each loading cycle. This increased rate of crack growth directly contributes to the broader spacing of striations observed in this region (figs. 4.16(d),4.17(d),4.18(d), 4.19(d) and 4.20(d)).

4.5.3 Conditional Elastic-Plastic (J_Q) fracture test

At the point where the crack becomes critical, the sample can no longer sustain the applied stress, leading to a final, often rapid fracture. This final fracture often occurs in a brittle or ductile manner and usually propagates in a direction that is generally perpendicular to the striations, which is aligned with the direction of the applied stress[104,147]. Fractography images of the final fracture zone is discussed below

Before P_{max}, 7075 Al alloy is showing smaller dimples with less pronounced fracture features (Fig.4.23), while after P_{max}, more prominent fracture features (Fig.4.24) with larger dimples are observed. Before P_{max} the sample is under increasing load, but the crack has not yet reached the point of maximum load-carrying capacity (P_{max})[59,147]. The material generally exhibits elastic or partially plastic deformation. The crack tip undergoes blunting, and crack initiation begins. However, the extent of crack

propagation is limited. The sample absorbs energy elastically and plastically, but fracture is not fully developed (Fig.4.23). Although there is a lot of stress and strain near the fracture tip, there isn't yet any noticeable crack growth. A comparatively tiny plastic zone starts to form close to the fracture tip [92]. Intergranular crack propagation and trans granular crack propagation can be seen in in 4.23(a) and 4.23(c) respectively because 4.23(a) is fractography image of SHT sample (having ductile dimples) and 4.23(c) is fractography of SHT+45% CR (having facets) sample[97,98].

After P_{max} the sample experiences plastic instability, leading to significant crack propagation and failure. At this stage, the sample cannot carry additional load, and the crack grows rapidly[98]. Crack propagation dominates, and the sample's fracture surface begins to exhibit more prominent features associated with rapid crack extension (e.g., dimples, facet and river like patterns). The sample dissipates energy largely through plastic deformation and crack propagation[97]. Since order of strength in all five conditions is SHT+PA+90% CR > SHT+PA > SHT+45% CR >SHT+ 60% WR > SHT sample (Fig.13). This explains why the fracture surfaces of the SHT condition and SHT+60% WR sample exhibit larger ductile dimples and void formations (figs. 4.23(a, d), 4.24(a, d)), indicative of ductile fracture [138,143]. In contrast, A mixed mode of ductile and brittle failure mechanisms is suggested by the fracture surface of the SHT+PA sample, which displays comparatively smaller dimples and areas of flat, trans granular cleavage with discrete facets (figs. 4.23(b), 4.24(b)) [95]. However, brittle fracture with facet and river-like patterns is seen in SHT+45% CR and SHT+PA+90% CR samples, respectively.